SFU HEP-131-96

Quarkonium spin structure in lattice NRQCD

Howard D. Trottier
*Department of Physics, Simon Fraser University, Burnaby, B.C., Canada V5A 1S6**
(November 1996)

arXiv:hep-lat/9611026v1 25 Nov 1996

Abstract

Numerical simulations of the quarkonium spin splittings are done in the framework of lattice nonrelativistic quantum chromodynamics (NRQCD). At leading order in the velocity expansion the spin splittings are of $O(M_Q v^4)$, where M_Q is the renormalized quark mass and v^2 is the mean squared quark velocity ($v^2_\psi \approx .3$ and $v^2_\Upsilon \approx .1$). A systematic analysis is done of all next-to-leading order corrections. This includes the addition of $O(M_Q v^6)$ relativistic interactions, and the removal of $O(a^2 M_Q v^4)$ discretization errors in the leading-order interactions. Simulations are done for both S- and P-wave mesons, with a variety of heavy quark actions and over a wide range of lattice spacings. Two prescriptions for the tadpole improvement of the action are also studied in detail: one using the measured value of the average plaquette, the other using the mean link measured in Landau gauge. Next-to-leading order interactions result in a very large reduction in the charmonium splittings, down by about 60% from their values at leading order. There are further indications that the velocity expansion may be poorly convergent for charmonium. Prelimary results show a small correction to the hyperfine splitting in the Upsilon system.

Typeset using REVTEX

*Email address: trottier@sfu.ca.

I. INTRODUCTION

Quarkonium physics has been the subject of renewed theoretical interest in recent years. The rich phenomenology of the charmonium and Upsilon families has spurred the development of nonrelativistic quantum chromodynamics (NRQCD), an effective field theory that relies on an expansion of the action in the mean squared velocity v^2 of the heavy quarks ($v_\psi^2 \approx .3$ and $v_\Upsilon^2 \approx .1$).

NRQCD has been formulated both on the lattice [1,2] and in the continuum [3]. Lattice simulations of the Upsilon and charmonium systems have recently been done by the NRQCD collaboration [4–8]. Results have also been reported for heavy-light [9] and $b\bar{c}$ spectra [7], and some unquenched simulations have also been done [8].

There are two key theoretical ingredients underlying lattice NRQCD calculations. One is an expansion of the effective action to a sufficient order in the heavy quark velocity, so as to obtain results of the desired accuracy. The other key ingredient is the use of tadpole renormalization [10] of the operators in the lattice action, which may then allow for reliable tree-level matching of the lattice theory with continuum QCD. A related problem is the development of sufficiently accurate discretizations of the relevant operators.

The quarkonium spin structure is particularly sensitive to the details of the NRQCD Hamiltonian. The Upsilon [5,7] and charmonium [6] spin splittings were recently analyzed to leaving order in v^2 by the NRQCD collaboration. At leading order in the velocity expansion the spin splittings are of $O(M_Q v^4)$, where M_Q is the renormalized quark mass. In the charmonium system however appreciable next-to-leading-order effects are expected, given the large mean squared velocity. Indeed a recent analysis of the charmonium hyperfine splitting using the relativistic Fermilab action gives a result (≈ 70 MeV) [11] that is significantly smaller than is obtained from leading-order NRQCD (≈ 96 MeV) [6].

In this paper a systematic analysis is done of all next-to-leading order corrections to the spin splittings. This includes the addition of $O(M_Q v^6)$ relativistic interactions, as well as the removal of $O(a^2 M_Q v^4)$ discretization errors that are present in the leading-order spin-dependent operators considered in Refs. [5–7].

Results from simulations with a variety of heavy quark actions and over a wide range of lattice spacings are presented for the charmonium S-wave hyperfine splitting. Some preliminary results are also reported for the charmonium P-wave fine structure, and for the Upsilon hyperfine splitting.

Furthermore two prescriptions for defining the tadpole improvement of the action are studied in detail: one using the measured value of the average plaquette, as considered in Refs. [5,6], the other using the mean link measured in Landau gauge. Landau gauge tadpole improvement has recently been shown to yield smaller discretization errors in the gluonic action (as measured by violations of rotational invariance in the heavy quark potential), compared to calculations using the average plaquette as input [12]. It is also interesting to note that the mean link is maximized in Landau gauge, so this prescription provides a lower bound on the tadpole renormalization compared to mean link determinations using other gauge fixings.

An important aspect of these simulations is the removal of leading discretization errors in the gluonic action as well as in the NRQCD action. Specifically, an $O(a^4)$-accurate gluonic action is used, together with $O(a^4)$-accurate clover fields and covariant derivatives

in the heavy quark action. Tadpole improvement of both the gluonic and the heavy quark actions has recently been shown to give a good description of the spin-averaged charmonium spectrum even on coarse lattices with spacings a as large as .4 fm [13]. In this paper the charmonium spin splittings are computed on lattices with spacings in the range of about .17 fm to .39 fm.

The next-to-leading order interactions are shown to result in a very large reduction in the charmonium hyperfine splitting, down by about 60% from the leading order result reported in Ref. [6] on a lattice of comparable spacing (when the same tadpole improvement scheme is used); results for the triplet P-wave meson masses show that the fine structure splittings are also reduced by about 60%. The next-to-leading order charmonium hyperfine splitting is about (55±5) MeV, compared to the relativistic Fermilab action result of about (70±3) MeV [11]. While the two calculations have different systematic errors, this comparsion suggests that further relativistic corrections, beyond the next-to-leading order considered here, are again very large.

These results indicate that the NRQCD velocity expansion may be poorly convergent for charmonium, with the first three terms in the expansion for the hyperfine splitting apparently oscillating in sign. Another possibility is that there are large radiative corrections to the coefficients of the spin-dependent operators in the effective action. Preliminary results for the Upsilon hyperfine splitting at next-to-leading order in v^2 (and with leading discretization errors removed) show little change from the leading-order result reported in Ref. [7].

The dependence of the hyperfine splitting on lattice spacing is also analysed. The splitting shows very little dependence on a when Landau gauge tadpole renormalization is used. The average plaquette tadpole scheme on the other hand has large discretization errors, but the results are not inconsistent with an extrapolation to the same splitting at zero lattice spacing in the two schemes. These results provide further support for the use of Landau gauge tadpole renormalization [12].

II. QUARK AND GAUGE-FIELD ACTIONS

The NRQCD effective action is based on power-counting rules for the magnitude of heavy quark and gauge field operators in quarkonium states. The expansion parameters are the mean squared velocity of the heavy quarks in the bound state, and the strong coupling constant. The coefficients of the operators in the effective action, to a given order in v^2, are determined by matching the predictions of NRQCD with those of full QCD [1,2].

The heavy quark lattice Hamiltonian is conveniently decomposed into the leading covariant kinetic energy operator H_0, plus relativistic and discretization corrections δH. Following Refs. [5,6], the quark Green function is given by

$$G_{t+1} = \left(1-\frac{aH_0}{2n}\right)^n U_4^\dagger \left(1-\frac{aH_0}{2n}\right)^n (1-a\delta H)\, G_t \quad (t>1), \tag{1}$$

where the initial evolution is set by

$$G_1 = \left(1-\frac{aH_0}{2n}\right)^n U_4^\dagger \left(1-\frac{aH_0}{2n}\right)^n \delta_{\vec{x},0}. \tag{2}$$

The kinetic energy operator H_0 is of $O(v^2)$, and is given by

$$H_0 = -\frac{\Delta^{(2)}}{2M_c^0}, \tag{3}$$

where M_c^0 is the bare quark mass and $\Delta^{(2)}$ is the lattice Laplacian. Relativistic corrections are organized in powers of the heavy quark velocity, with terms up to $O(v^6)$ considered here:

$$\delta H = \delta H^{(4)} + \delta H^{(6)}. \tag{4}$$

Simulations with the complete set of $O(v^4)$ corrections were reported in Refs. [5,6]:

$$\begin{aligned}\delta H^{(4)} = &-c_1\frac{(\Delta^{(2)})^2}{8(M_c^0)^3} + c_2\frac{ig}{8(M_c^0)^2}(\tilde{\boldsymbol{\Delta}}\cdot\tilde{\mathbf{E}} - \tilde{\mathbf{E}}\cdot\tilde{\boldsymbol{\Delta}}) \\ &-c_3\frac{g}{8(M_c^0)^2}\boldsymbol{\sigma}\cdot(\tilde{\boldsymbol{\Delta}}\times\tilde{\mathbf{E}} - \tilde{\mathbf{E}}\times\tilde{\boldsymbol{\Delta}}) - c_4\frac{g}{2M_c^0}\boldsymbol{\sigma}\cdot\tilde{\mathbf{B}} \\ &+c_5\frac{a^2\Delta^{(4)}}{24M_c^0} - c_6\frac{a(\Delta^{(2)})^2}{16n(M_c^0)^2}.\end{aligned} \tag{5}$$

The first two terms in $\delta H^{(4)}$ are spin-independent relativistic corrections, and the last two terms come from finite lattice spacing corrections to the lattice Laplacian and the lattice time derivative respectively. The parameter n is introduced to remove instabilities in the heavy quark propagator caused by the highest momentum modes of the theory [2].

While $\delta H^{(4)}$ yields spin-averaged spectra to next-to-leading order in the velocity expansion, it contains only leading order spin-dependent interactions. In potential model language the third term above (c_3) generates the spin-orbit and tensor potentials which drive the P-wave fine structure, while the fourth term (c_4) generates the color-magnetic S-wave hyperfine splitting.

Spin-dependent interactions at $O(v^6)$ were derived in Ref. [2]:

$$\begin{aligned}\delta H^{(6)} = &-c_7\frac{g}{8(M_c^0)^3}\left\{\tilde{\Delta}^{(2)}, \boldsymbol{\sigma}\cdot\tilde{\mathbf{B}}\right\} \\ &-c_8\frac{3g}{64(M_c^0)^4}\left\{\tilde{\Delta}^{(2)}, \boldsymbol{\sigma}\cdot(\tilde{\boldsymbol{\Delta}}\times\tilde{\mathbf{E}} - \tilde{\mathbf{E}}\times\tilde{\boldsymbol{\Delta}})\right\} \\ &-c_9\frac{ig^2}{8(M_c^0)^3}\boldsymbol{\sigma}\cdot\tilde{\mathbf{E}}\times\tilde{\mathbf{E}}.\end{aligned} \tag{6}$$

Notice the field strength bilinear (c_9), which is peculiar to the nonAbelian theory. There are additional $O(v^6)$ terms which contribute to spin-averaged spectra; these are not considered here.

The derivative operators and the fields are evaluated with their leading discretization errors removed, in order to minimize the effects of lattice artifacts on the spin splittings. This is indicated by the tilda superscripts on these operators in Eqs. (5) and (6). At leading order in a the action of the symmetric lattice derivative Δ_i is defined by

$$a\Delta_i G(x) \equiv \tfrac{1}{2}[U_i(x)G(x+a\hat{\imath}) - U_i^\dagger(x-a\hat{\imath})G(x-a\hat{\imath})]. \tag{7}$$

At tree level the $O(a^4)$-accurate derivative operator $\tilde{\Delta}_i$ that is used in Eqs. (5) and (6) is given by [2]

$$\tilde{\Delta}_i = \Delta_i - \frac{a^2}{6}\Delta_i^{(+)}\Delta_i\Delta_i^{(-)}, \tag{8}$$

where $\Delta_i^{(+)}$ and $\Delta_i^{(-)}$ are leading-order forward and backward covariant finite differences:

$$\begin{aligned} a\Delta_i^{(+)}G(x) &\equiv U_i(x)G(x+a\hat{\imath}) - G(x), \\ a\Delta_i^{(-)}G(x) &\equiv G(x) - U_i^\dagger(x-a\hat{\imath})G(x-a\hat{\imath}). \end{aligned} \tag{9}$$

At leading-order in a the lattice Laplacian $\Delta^{(2)}$ is expressed in terms of covariant second order differences

$$\Delta^{(2)} = \sum_i \Delta_i^{(2)}, \tag{10}$$

where

$$a^2\Delta_i^{(2)}G(x) = U_i(x)G(x+a\hat{\imath}) - 2G(x) + U_i^\dagger(x-a\hat{\imath})G(x-a\hat{\imath}). \tag{11}$$

The $O(a^4)$-accurate Laplacian $\tilde{\Delta}^{(2)}$ is used in Eq. (6), and at tree-level is given by [2]

$$\tilde{\Delta}^{(2)} = \Delta^{(2)} - \frac{a^2}{12}\Delta^{(4)}, \tag{12}$$

where

$$\Delta^{(4)} = \sum_i \left(\Delta_i^{(2)}\right)^2 \tag{13}$$

is a lattice representation of the continuum operator $\sum_i D_i^4$. Note that discretization errors in H_0 have been removed in this way by the addition of the c_5 term in Eq. (5). What is new in the present work is the removal of discretization errors in the leading order P-wave interaction (c_3), and the Darwin term (c_2), as well as the addition of the $O(v^6)$ spin terms in Eq. (6).

To complete the removal of discretization errors from the spin-dependent interactions $O(a^4)$-accurate chromo-electric and -magnetic fields have been used in these simulations. In Refs. [5,6] the leading order field strength $F_{\mu\nu}$ was evaluated using the standard traceless clover operator:

$$F_{\mu\nu}(x) = \frac{1}{2i}\left(\Omega_{\mu\nu}(x) - \Omega_{\mu\nu}^\dagger(x)\right) - \frac{1}{3}\mathrm{Im}\left(\mathrm{Tr}\,\Omega_{\mu\nu}(x)\right), \tag{14}$$

where $\Omega_{\mu\nu}$ is an average over the 4 counterclockwise plaquettes in the (μ,ν) plane containing the site x

$$\Omega_{\mu\nu} = -\frac{1}{4}\sum_{\alpha=\pm\mu}\sum_{\beta=\pm\nu} U_\alpha(x)U_\beta(x+\hat{\alpha})U_{-\alpha}(x+\hat{\alpha}+\hat{\beta})U_{-\beta}(x+\hat{\beta}). \tag{15}$$

The $O(a^4)$-accurate field strength $\tilde{F}_{\mu\nu}$ used here is computed following the analysis of Ref. [2]:

$$\tilde{F}_{\mu\nu}(x) = \frac{5}{3}F_{\mu\nu}(x) - \frac{1}{6}\Big[U_\mu(x)F_{\mu\nu}(x+\hat{\mu})U_\mu^\dagger(x) + U_\mu^\dagger(x-\hat{\mu})F_{\mu\nu}(x-\hat{\mu})U_\mu(x-\hat{\mu}) - (\mu \leftrightarrow \nu)\Big]. \quad (16)$$

The "improved" chromo-electric and -magnetic fields are defined in terms of the field strength, $\tilde{E}_i = \tilde{F}_{4i}$ and $\tilde{B}_i = \frac{1}{2}\epsilon_{ijk}\tilde{F}_{jk}$.

It should be noted that some of the discretization errors that are removed by using $\tilde{\Delta}$, $\tilde{\Delta}^{(2)}$, and $\tilde{F}_{\mu\nu}$ in Eqs. (5) and (6), in place of their leading order counterparts, may in fact be comparable to or smaller than higher order relativistic corrections that are not included here. This includes for example the use of $\tilde{\Delta}^{(2)}$ and $\tilde{F}_{\mu\nu}$ in the $O(v^6)$ terms in Eq. (6), and the use of the improved operators in the Darwin term (c_2). On the other hand, the use of improved operators in the leading spin-dependent interactions (c_3 and c_4) corrects for errors of $O(a^2 M_c v^4)$ in the spin splittings which, for the range of lattice spacings studied here, may be comparable to the $O(M_c v^6)$ contributions from $\delta H^{(6)}$.

At tree-level all of the coefficients c_i in Eqs. (5) and (6) are one. However, very large radiative corrections in the lattice theory can arise from tadpoles that are induced by the nonlinear connection between the link variables U_μ and the continuum gauge fields. Most of the effects of tadpoles can be removed by a mean-field renormalization of the link [10]:

$$U_\mu(x) \to \frac{U_\mu(x)}{u_0}. \quad (17)$$

The links are rescaled in the simulation before they are input to the quark propagator subroutine, to be sure that Eq. (17) is correctly implemented in all terms in the heavy quark action.

In most previous work the fourth root of the average plaquette has been used to set the value of u_0:

$$u_{0,P} \equiv \left\langle \tfrac{1}{3}\mathrm{ReTr}\, U_{\rm pl} \right\rangle^{1/4}. \quad (18)$$

Simulations were done here with this renormalization prescription. In addition, simulations were also done using the mean link in Landau gauge to set u_0, as recently suggested by Lepage [12]

$$u_{0,L} \equiv \left\langle \tfrac{1}{3}\mathrm{ReTr}\, U_\mu \right\rangle, \quad \partial_\mu A_\mu = 0, \quad (19)$$

where a standard lattice implementation of the continuum Landau gauge fixing is used [14] (it was found that the removal of leading discretization errors in the lattice version of $\partial_\mu A_\mu = 0$ results in a negligible change to the value of $u_{0,L}$).

Finally, the gauge-field configurations were generated using an $O(a^4)$-accurate tadpole-improved action [13]

$$S[U] = \beta \sum_{\rm pl} \tfrac{1}{3}\mathrm{ReTr}\left(1 - U_{\rm pl}\right) - \frac{\beta}{20u_0^2}\sum_{\rm rt} \tfrac{1}{3}\mathrm{ReTr}\left(1 - U_{\rm rt}\right), \quad (20)$$

where the sums are over all oriented 1×1 plaquettes and 1×2 rectangles.

III. MESON PROPAGATORS

In order to increase the overlap of the meson propagators with the ground states of interest here, a gauge-covariant smearing procedure has been used [15]. A meson creation operator is constructed from quark and antiquark creation operators $\psi^\dagger$ and $\chi^\dagger$ [1,5,6]:

$$\sum_{\vec{x}} \psi^\dagger(\vec{x})\Gamma(\vec{x})\chi^\dagger(\vec{x}), \tag{21}$$

with

$$\Gamma(\vec{x}) \equiv \Omega(\vec{x})\gamma(\vec{x}), \tag{22}$$

where $\Omega(\vec{x})$ is a 2×2 matrix in spin-space, with derivative operator entries, which gives the quantum numbers of the state of interest. $\gamma(\vec{x})$ is a gauge-covariant local smearing operator, which is taken to have the simple form [15]

$$\gamma(\vec{x}) = \left(1 + \epsilon\Delta^{(2)}(\vec{x})\right)^{n_s} \tag{23}$$

(an invariant under the lattice cubic group). The weight ϵ and the number of smearing iterations n_s are adjusted to optimize the overlap with the ground state.

The meson correlation function $G_{\rm meson}$ at zero momentum is then given by

$$G_{\rm meson}(\vec{p}=0,t) = \sum_{\vec{y}} {\rm Tr}\left[G_t^\dagger(\vec{y}-\vec{x})\Gamma^\dagger_{(sk)}(\vec{y})G_t(\vec{y}-\vec{x})\Gamma_{(sc)}(\vec{x})\right], \tag{24}$$

where different smearing parameters may be used at the source and sink, and where a single spatial origin $\vec{x}$ for the meson propagator was generally used. Finite momentum propagators for the ${}^1S_0$ were analyzed using a local δ-function source and sink:

$$G_{\rm meson}(\vec{p},t) = \sum_{\vec{y}} {\rm Tr}\left[G_t^\dagger(\vec{y}-\vec{x})G_t(\vec{y}-\vec{x})\right] e^{-i\vec{p}\cdot(\vec{y}-\vec{x})}. \tag{25}$$

Correlation functions were computed for the ${}^1S_0$ ($\Omega = I$), ${}^3S_1$ ($\Omega = \sigma_i$) and ${}^1P_1$ ($\Omega = \Delta_i$) mesons. The three triplet P-wave correlators (${}^3P_0$, ${}^3P_1$, ${}^3P_2$) were also analyzed; the relevant operators Ω for these states are tabulated in Ref. [5]. Only selected meson polarizations were used. Propagators were generated for all (equal) quark-antiquark colors but, in order to save computer time, the initial quark and antiquark spins were set to 1. The ${}^3S_1z$ and ${}^1S_0$ states were thus obtained from a single propagator, since the 1×1 component of the spin matrix Ω is the same for both states [5]. All three polarizations of the ${}^1P_1$ were generated, but only one from each of the ${}^3P_1$ and ${}^3P_2$.

IV. RESULTS

Three lattices were generated using the mean link in Landau gauge to set the tadpole factor ($u_{0,L}$) and four lattices with comparable spacings were generated using the average plaquette tadpole ($u_{0,P}$). The parameters of these seven lattices are given in Tables I and II. In order to distinguish between the two sets of simulations, β_L is used to denote the lattice

coupling when Landau-gauge tadpole renormalization is used, and β_P when the average plaquette is used.

A standard Cabbibo-Marinari pseudo-heat bath was used to generated the gauge field configurations. Integrated autocorrelation times $\tau_{\rm int}$ were checked for all correlation functions, and were found to be remarkably short; 10 updates between measurements yields $\tau_{\rm int} \lesssim 0.5$ on the three lattices with $a \lesssim .2$ fm, and on the coarser lattices 5 updates was found to be sufficient.

Smeared-smeared correlators were used for the P-waves, while local sources and smeared sinks were used for the S-waves. Ten smearing iterations [$n_s = 10$ in Eq. (23)] were used for the three lattices with $a \lesssim .2$ fm, 5 iterations for the lattices with a near .28 fm, and 2 iterations for the lattices with $a \approx .39$ fm. A smearing weight $\epsilon = 1/12$ was used in all cases.

The lattice spacings are determined from the spin-averaged $1P - 1S$ mass difference, following Refs. [5,6]. This mass difference is known to be independent of the quark mass in the charm to bottom region. For this purpose the singlet ${}^1P_1$ and the spin-averaged ${}^3S_1$, ${}^1S_0$ masses were used. The simulation results for the splitting were fixed to the experimental value for charmonium of 458 MeV.

After the lattice spacing was extracted, the kinetic mass $M_{\rm kin}$ (in physical units) of the ${}^1S_0$ state was determined by fitting the energy $E_{\mathbf{P}}$ of the boosted state to the form

$$E_{\mathbf{P}} - E_0 = \frac{\mathbf{P}^2}{2M_{\rm kin}}. \tag{26}$$

Fits were made to the state with momentum components $(1,0,0)$ in units of $2\pi/(Na)$; in some cases simultaneous fits including states with momentum components $(1,1,0)$ and $(1,1,1)$ were also done, with little change to the fit values of $M_{\rm kin}$. A dispersion relation including relativistic corrections [5,6] was also tried, and the resulting changes to the fit values of $M_{\rm kin}$ were within a few percent, as expected on these lattices.

The correct values of the bare charm mass M_c^0 were determined by tuning so that $M_{\rm kin}$ agrees with the experimental value of the mass of the η_c (2.98 GeV). The bare masses are listed in Tables I and II, and all yield $M_{\rm kin} = 2.9(1)$ GeV. For bare masses $aM_c^0 < 1.2$ a stability parameter $n = 4$ was used in the quark propagators, Eqs. (1) and (2); for $1.2 < aM_c^0 < 1.5$ $n = 3$ was used, and for the larger bare masses $n = 2$ was used.

Effective mass plots $m_{\rm eff}(T) = -\log(G(T)/G(T-1))$ for several lattices are shown in Figures 1–4, using jackknife errors. Single exponential fits to the correlation functions are used to get the best estimates of the masses of the individual states. The fitting procedure included the full covariance matrix for the data, using the svd algorithm [16]. The correlation functions for states of a given partial wave are highly correlated; following Refs. [5,6] a spin splitting δE was obtained from a correlated fit of the form

$$\begin{aligned} G_{\rm meson,A}(t) &= c_A e^{-E_A t}, \\ G_{\rm meson,B}(t) &= c_B e^{-(E_A+\delta E)t}. \end{aligned} \tag{27}$$

Detailed fit results for several lattices are reported in Tables III–VI. The statistical errors were estimated using bootstrap ensembles of 1000 samples. Final estimates of the dimensionless energies are obtained from these fits by finding two or three successive $t_{\rm min}/t_{\rm max}$

intervals for which the fit results overlap within statistical errors; acceptable Q values were obtained in all cases at these $t_{\rm min}/t_{\rm max}$ values. Estimates of the systematic errors in the final fit results are taken from the largest statistical errors in the overlapping intervals.

The final fit results are shown in Tables VII and VIII, where the resulting lattice spacings and hyperfine splittings in physical units are also given. The dominant error in the splitting comes from the systematic error in the determination of the bare quark mass. The error in the mass comes in part from the uncertainty in a^{-1}, which has been included in the error estimates for the splittings in physical units; however, there is a further systematic error of order 10% in the quark mass determination, coming from higher order (spin-independent) relativistic corrections [6].

V. DISCUSSION

The hyperfine splittings are plotted as a function of lattice spacing in Fig. 5, where the results from the relativistic Fermilab action [11] and the leading order NRQCD calculation [6] are included. Some coarse lattice results from the tadpole-improved relativistic D234 [17] action are also shown.

The next-to-leading order corrections result in a very large reduction in the hyperfine splitting, down by about 60% from the leading order result on a lattice of comparable spacing, when the same plaquette tadpole renormalization scheme ($u_{0,P}$) is used in both cases.

The hyperfine splitting shows very little a dependence when the Landau gauge tadpole scheme $u_{0,L}$ is used. The results with $u_{0,P}$ on the other hand have large discretization errors, which prevents a reliable extrapolation to zero lattice spacing in this case; however, the results are not inconsistent with an extrapolation to the same splitting as is obtained with Landau gauge $u_{0,L}$.

From these results the hyperfine splitting at next-to-leading order in the velocity expansion, and at zero lattice spacing, can be estimated at roughly (55 ± 5) MeV. This can be compared with the Fermilab action result of approximately (70 ± 3) MeV [11]. While the two calculations have different systematic errors, this suggests that further relativistic corrections, beyond the next-to-leading-order considered here, are again very large. [The experimental value is (118 ± 2) MeV, which indicates that there are significant effects due to quenching [11,6].]

These considerations are supported by results obtained here for the triplet P-wave spectra ($^3P_0$, $^3P_1$, $^3P_2$). The next-to-leading order fine structure splittings are apparently very small, and much better statistics are required for an accurate determination. Simulations with $u_{0,L}$ give a $^3P_2 - {}^3P_0$ splitting of about (30 ± 15) MeV, down by about 60% from the leading-order result of (110 ± 10) MeV reported in Ref. [6] (the experimental value is (141 ± 10) MeV). The next-to-leading order fine structure splittings with $u_{0,P}$ are even harder to measure, but the results suggest that the splittings may actually be in the wrong order with that tadpole scheme (as least in the range of lattice spacings analyzed here).

These results indicate that the NRQCD velocity expansion for charmonium may be poorly convergent, with the first three terms in the expansion for the hyperfine splitting apparently oscillating in sign. However there are other sources of systematic error in the

NRQCD action which must also be considered. Radiative corrections to the operator coefficients c_3 and c_4 in Eq. (5) are of particular importance.

It is worthwhile to assess the relative importance of the various next-to-leading order corrections that have been considered here. Within a given tadpole renormalization scheme the most important correction for the charmonium system comes from the relativistic spin-dependent interactions $\delta H^{(6)}$ [Eq. (6)], and these drive the large reduction in the splittings. There is some indication that the field strength bilinear (term c_9) plays a relatively small role in these effects. The use of $O(a^4)$-accurate clover fields increases the spin splittings, a correction amounting to about 20% of the $O(a^2)$-accurate splittings on the coarsest lattices considered here (this correction falls below about 10% at the smallest spacings).

The effect of a change in the tadpole renormalization scheme is very significant. The spin splittings vary as $1/u_0^4$ due to the renormalization of the clover field interactions (except for the field strength bilinear, which varies as $1/u_0^8$). This renormalization causes most of the change due to tadpole scheme, as can be seen from the values of $u_{0,L}$ and $u_{0,P}$ in Tables I and II (additional changes in the splittings are presumably caused by the renormalization of the gluonic action). For example, at $a \approx .18$ fm the ratio $(u_{0,P}/u_{0,L})^4$ is about 1.2, and at $a \approx .39$ fm the ratio is about 1.5.

Relativistic corrections are expected to be much smaller for the Upsilon system. Preliminary results from a next-to-leading order calculation at $\beta_P = 7.2$ give an $\Upsilon - \eta_b$ hyperfine splitting of (22.4 ± 1.3) MeV, using a bare mass $aM_b^0 = 3.15$. This is within errors of the leading-order result reported in Ref. [7] on a lattice with comparable spacing (using $u_{0,P}$), which is consistent with the velocity expansion, given the fact that $v_\Upsilon^2 \approx 0.1$. The small size of the net correction, relative to the charmonium system, also appears to be driven by a near cancellation of the $O(a^2 M_Q v^4)$ discretization corrections (which tend to raise the splittings) and the $O(M_Q v^6)$ relativistic corrections (which tend to lower them), which are much closer in magnitude in the Upsilon system. This was demontrated by doing a calculation with a Wilson gauge field action at $\beta = 5.7$, without removing discretization errors in the clover field, but including the $O(M_Q v^6)$ relativistic interactions; this results in a reduction of the Upsilon hyperfine splitting by about 15% compared to the leading order calculation [7] at the same β.

It is also interesting to note that the lattice spacing as determined from the $1P - 1S$ splitting is different for Upsilon and charmonium. At $\beta_P = 7.2$ preliminary results give $a_\Upsilon = 0.146(9)$ fm, compared to $a_\psi = 0.171(4)$ fm. This is comparable to the difference between the two determinations of the spacing in Ref. [7].

VI. SUMMARY AND OUTLOOK

It has been shown that spin-dependent interactions at next-to-leading order in the NRQCD velocity expansion yield very large corrections to the charmonium spin splittings, down by about 60% from their values at leading order (when the same tadpole-improvement scheme is used on lattices with comparable spacings). There are indications that further relativistic corrections for charmonium are also very large. The corrections to the hyperfine splitting in the Upsilon system are small. More work needs to be done in order to assess the validity of the NRQCD effective action in simulations of charmonium, including better measurements of the triplet P-wave spectra. Estimates of the radiative corrections to the

operator coefficients in the heavy quark action are also needed. More complete calculations of the Upsilon splittings would also provide useful information. The results obtained here provide further support for the use of Landau gauge tadpole renormalization.

ACKNOWLEDGMENTS

I am indebted to G. P. Lepage and R. M. Woloshyn for many helpful discussions and suggestions. I also thank C. Davies, J. Shigemitsu and J. Sloan for useful conversations. This work was supported in part by the Natural Sciences and Engineering Research Council of Canada.

REFERENCES

[1] G. P. Lepage and B. A. Thacker, Nucl. Phys. B (Proc. Suppl.) **4**, 199 (1988); B. A. Thacker and G. P. Lepage, Phys. Rev. D **43**, 196 (1991).

[2] G. P. Lepage, L. Magnea, C. Nakhleh, U. Magnea and K. Hornbostel, Phys. Rev. D **46**, 4052 (1992).

[3] G. T. Bodwin, E. Braaten, G. P. Lepage, Phys. Rev. D **51**, 1125 (1995).

[4] C. T. H. Davies, K. Hornbostel, A. Langnau, G. P. Lepage, A. Lidsey, C. J. Morningstar, J. Shigemitsu and J. Sloan, Phys. Rev. Lett. **73**, 2654 (1994).

[5] C. T. H. Davies, K. Hornbostel, A. Langnau, G. P. Lepage, A. Lidsey, J. Shigemitsu and J. Sloan, Phys. Rev. D **50**, 6963 (1994).

[6] C. T. H. Davies, K. Hornbostel, G. P. Lepage, A. Lidsey, J. Shigemitsu and J. Sloan, Phys. Rev. D**52**, 6519 (1995).

[7] C. T. H. Davies, K. Hornbostel, A. Langnau, G. P. Lepage, A. Lidsey, J. Shigemitsu and J. Sloan, Nucl. Phys. B (Proc. Suppl.) **47**, 421 (1996).

[8] For a recent review see J. Shigemitsu, Report No. hep-lat/9608058.

[9] A. Ali Khan, C. T. H. Davies, S. Collins, J. Sloan and J. Shigemitsu, Phys. Rev. D **53**, 6433 (1996).

[10] G. P. Lepage and P. B. Mackenzie, Phys. Rev. D **48**, 2250 (1993).

[11] A. El-Khadra and B. Mertens, Nucl. Phys. B (Proc. Suppl.) **42**, 406 (1995); A. El-Khadra, Nucl. Phys. B (Proc. Suppl.) **26**, 372 (1992). More recent results are reviewed in Ref. [8].

[12] G. P. Lepage, private communication (1996).

[13] M. Alford, W. Dimm, G. P. Lepage, G. Hockney, and P. B. Mackenzie, Phys. Lett. **B361**, 87 (1995).

[14] See for example C. T. H. Davies *et al.*, Phys. Rev. D **37**, 1581 (1988).

[15] G. P. Lepage, private communication (1996).

[16] I thank R. M. Woloshyn for providing me with a copy of his svd fitting routines.

[17] M. G. Alford, T. R. Klassen and G. P. Lepage, Report No. hep-lat/9608113.

TABLES

β_L	$\langle\frac{1}{3}\mathrm{ReTr}\,U_\mu\rangle$	$\langle\frac{1}{3}\mathrm{ReTr}\,U_{\mathrm{pl}}\rangle^{1/4}$	a (fm)	aM_c^0	Volume	N_{meas}
7.4	.829	.875	.18	1.18	$10^3 \times 16$	752
7.0	.780	.850	.28	1.90	$6^3 \times 10$	1740
6.6	.743	.825	.39	2.65	$6^3 \times 10$	2092

TABLE I. Simulation parameters using the Landau gauge mean link to determine the tadpole renormalization, $u_{0,L} = \langle\frac{1}{3}\mathrm{ReTr}\,U_\mu\rangle$ (second column). N_{meas} is the number of configurations used for propagator measurements.

β_P	$\langle\frac{1}{3}\mathrm{ReTr}\,U_\mu\rangle$	$\langle\frac{1}{3}\mathrm{ReTr}\,U_{\mathrm{pl}}\rangle^{1/4}$	a (fm)	aM_c^0	Volume	N_{meas}
7.2	.834	.874	.17	0.81	$10^3 \times 16$	474
7.0	.810	.865	.21	1.10	$8^3 \times 10$	923
6.8	.786	.854	.26	1.43	$6^3 \times 10$	1815
6.25	.738	.821	.39	2.30	$6^3 \times 10$	2841

TABLE II. Simulation parameters using the average plaquette to determine the tadpole renormalization, $u_{0,P} = \langle\frac{1}{3}\mathrm{ReTr}\,U_{\mathrm{pl}}\rangle^{1/4}$ (third column).

$t_{\mathrm{min}}/t_{\mathrm{max}}$	$^1P_1$	$^3S_1$	$^1S_0$	$^3S_1 - {}^1S_0$
2/16	0.735(5)	0.298(2)	0.242(1)	0.0537(6)
3/16	0.715(6)	0.293(2)	0.239(1)	0.0533(5)
4/16	0.709(9)	0.289(2)	0.237(1)	0.0518(6)
5/16	0.694(12)	0.286(2)	0.235(1)	0.0506(6)
6/16	0.688(16)	0.285(2)	0.235(1)	0.0497(7)
7/16	0.672(23)	0.284(2)	0.234(1)	0.0500(8)
8/16	0.661(30)	0.284(2)	0.234(1)	0.0498(9)
9/16	0.700(51)	0.284(2)	0.234(1)	0.0494(10)

TABLE III. Examples of fits to Landau-gauge tadpole simulation at $\beta_L = 7.4$ ($a = .18$ fm). Single exponential fits were used for each individual state, and a correlated δE fit for the $^3S_1$ and $^1S_0$ was used to get the hyperfine splitting.

$t_{\rm min}/t_{\rm max}$	$^1P_1$	$^3S_1$	$^1S_0$	$^3S_1 - {}^1S_0$
2/10	1.280(8)	0.404(1)	0.304(1)	0.0980(6)
3/10	1.268(15)	0.395(1)	0.299(1)	0.0969(6)
4/10	1.279(35)	0.393(1)	0.298(1)	0.0950(7)
5/10	1.198(71)	0.392(2)	0.298(1)	0.0945(7)
6/10	1.18(14)	0.392(2)	0.298(1)	0.0946(10)
7/10	1.44(43)	0.392(2)	0.298(1)	0.0944(12)

TABLE IV. Examples of fits to Landau-gauge tadpole simulation at $\beta_L = 6.6$ ($a = .39$ fm). Fits were done as in Table III.

$t_{\rm min}/t_{\rm max}$	$^1P_1$	$^3S_1$	$^1S_0$	$^3S_1 - {}^1S_0$
2/16	1.120(6)	0.715(2)	0.675(2)	0.0399(5)
3/16	1.101(7)	0.708(2)	0.670(2)	0.0395(5)
4/16	1.089(9)	0.706(2)	0.669(2)	0.0369(5)
5/16	1.083(12)	0.704(2)	0.667(2)	0.0363(6)
6/16	1.087(15)	0.702(2)	0.667(2)	0.0357(7)
7/16	1.083(21)	0.700(2)	0.666(2)	0.0352(7)
8/16	1.093(29)	0.701(2)	0.666(2)	0.0352(8)

TABLE V. Examples of fits to average plaquette tadpole simulation at $\beta_P = 7.2$ ($a = .17$ fm). Fits were done as in Table III.

$t_{\rm min}/t_{\rm max}$	$^1P_1$	$^3S_1$	$^1S_0$	$^3S_1 - {}^1S_0$
2/10	1.773(7)	0.858(1)	0.801(1)	0.0575(3)
3/10	1.754(14)	0.853(1)	0.797(1)	0.0570(3)
4/10	1.754(26)	0.852(1)	0.795(1)	0.0565(3)
5/10	1.771(60)	0.851(1)	0.795(1)	0.0561(4)
6/10		0.851(1)	0.795(1)	0.0560(4)
7/10		0.850(1)	0.795(1)	0.0556(6)

TABLE VI. Examples of fits to average plaquette tadpole simulation at $\beta_P = 6.25$ ($a = .39$ fm). Fits were done as in Table III.

β_L	$^1P_1$	$^1S_0$	$^3S_1 - {}^1S_0$	a (fm)	Hyperfine (MeV)
7.4	0.68(2)	0.234(1)	0.0497(7)	0.176(9)	55.7(27)
7.0	1.01(2)	0.305(1)	0.0772(8)	0.278(9)	54.6(18)
6.6	1.27(3)	0.298(1)	0.0945(7)	0.388(13)	48.0(17)

TABLE VII. Final fit results for the dimensionless energies from Landau-gauge tadpole simulations; the resulting lattice spacings and hyperfine splittings in physical units are also shown. The quoted errors in the hyperfine splittings in physical units include the systematic errors in a.

β_P	$^1P_1$	$^1S_0$	$^3S_1 - {}^1S_0$	a (fm)	Hyperfine (MeV)
7.2	1.09(1)	0.666(2)	0.0352(7)	0.171(4)	40.5(13)
7.0	1.23(2)	0.728(2)	0.0354(7)	0.205(9)	34.1(16)
6.8	1.42(2)	0.790(2)	0.0427(6)	0.257(9)	32.7(12)
6.25	1.75(3)	0.795(1)	0.0560(6)	0.393(13)	28.1(10)

TABLE VIII. Final fit results from average plaquette simulations.

FIGURES

FIG. 1. Effective mass plot for $\beta_L = 7.4$ ($a = .18$ fm): $^1P_1$ state ($\Box$) and $^1S_0$ state ($\circ$).

FIG. 2. Effective mass plot for $\beta_L = 6.6$ ($a = .39$ fm): $^1P_1$ state ($\Box$) and $^1S_0$ state ($\circ$).

FIG. 3. Effective mass plot for $\beta_P = 7.2$ ($a = .17$ fm): $^1P_1$ state ($\Box$) and $^1S_0$ state ($\circ$).

FIG. 4. Effective mass plot for $\beta_P = 6.25$ ($a = .39$ fm): $^1P_1$ state ($\Box$) and $^1S_0$ state ($\circ$).

FIG. 5. Hyperfine splittings versus lattice spacing squared. The next-to-leading order NRQCD results with Landau gauge tadpoles ($\blacksquare$) and with average plaquette tadpoles ($\circ$) are shown, as well as the leading-order result ($\times$) from Ref. [6]. Also shown are results obtained with the relativistic Fermilab action ($\Box$) [11], and coarse lattice results from the relativistic tadpole-improved D234 action ($\triangle$) [17]. The experimental value is (118 ± 2) MeV.

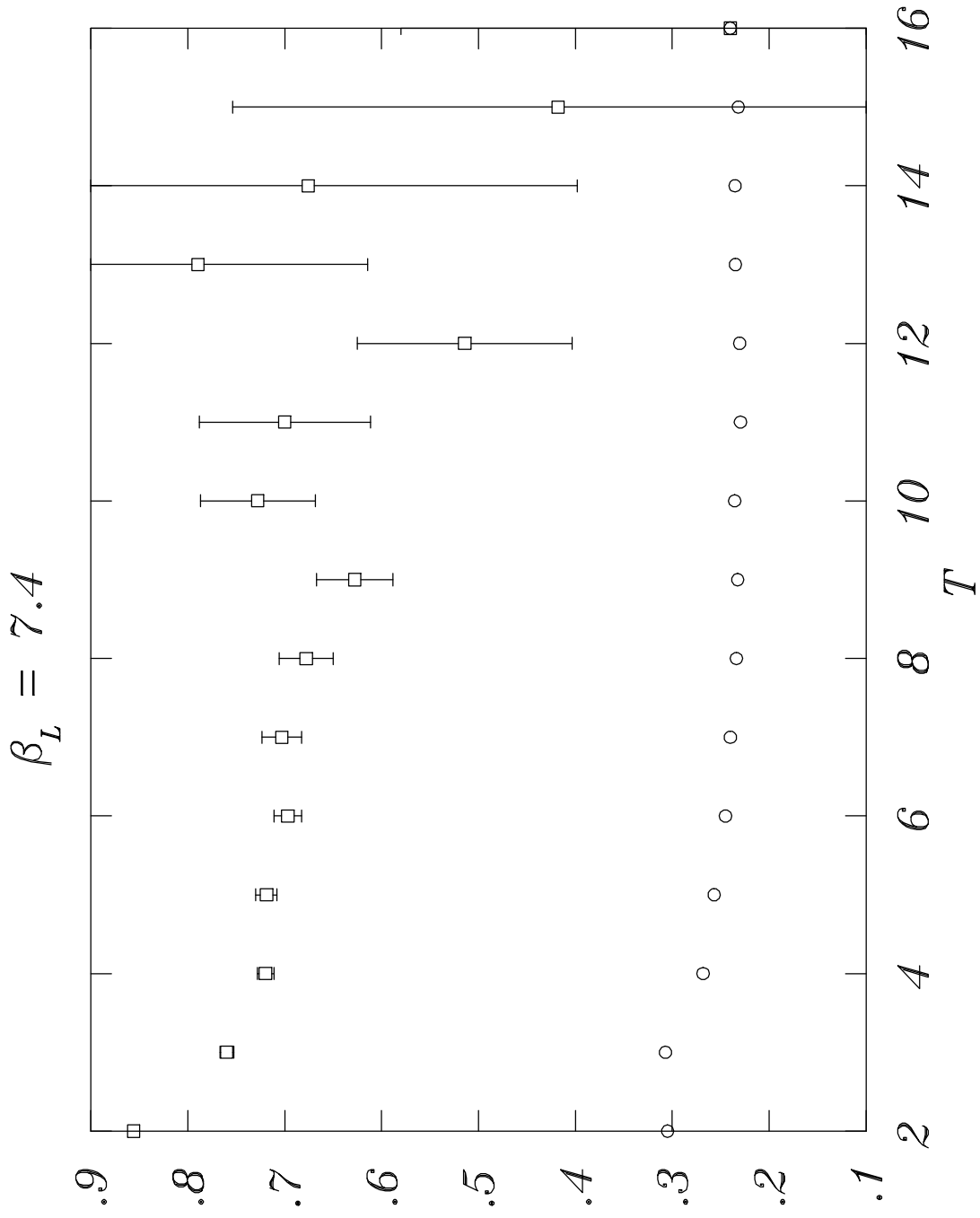

Figure 1

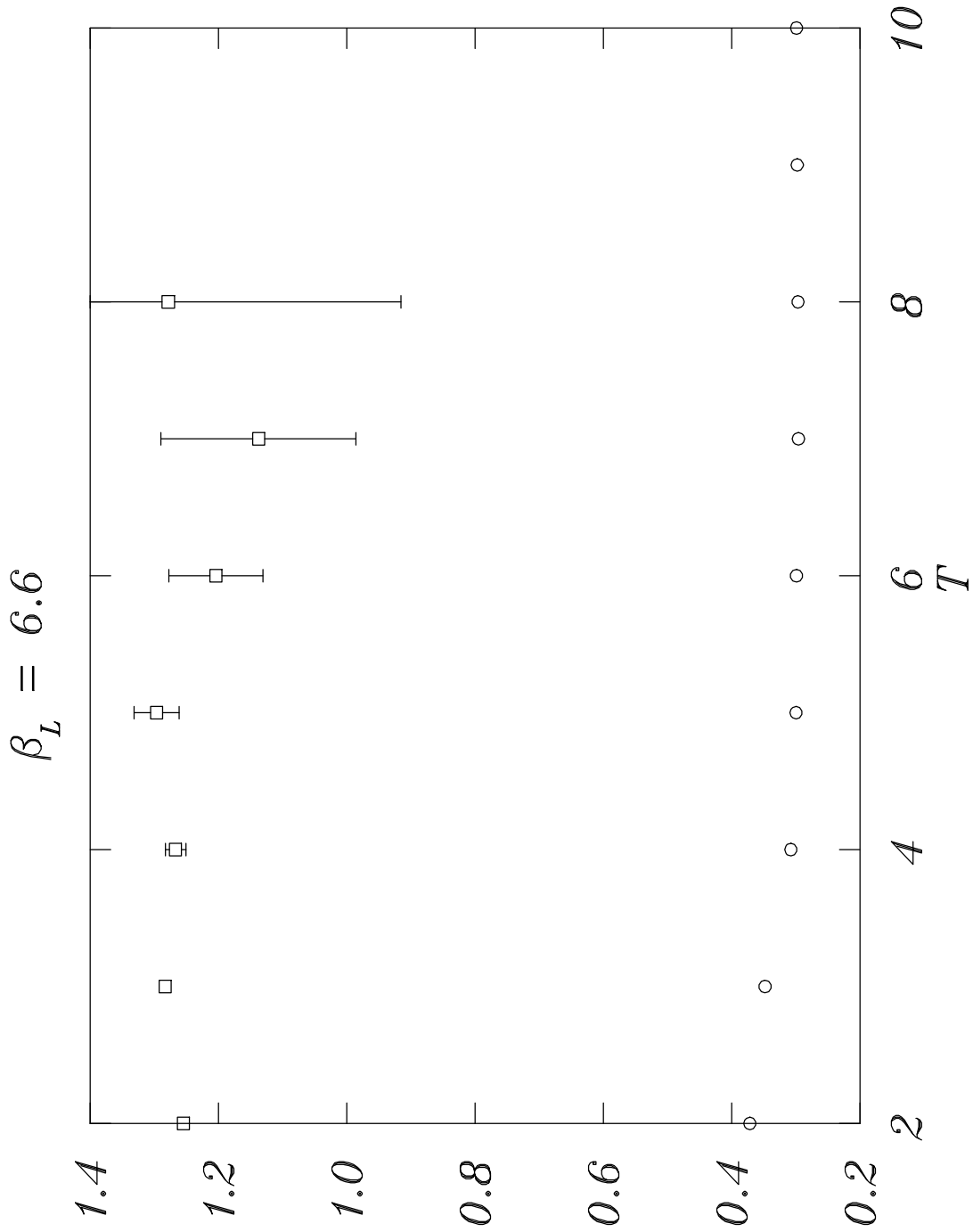

Figure 2

Figure 3

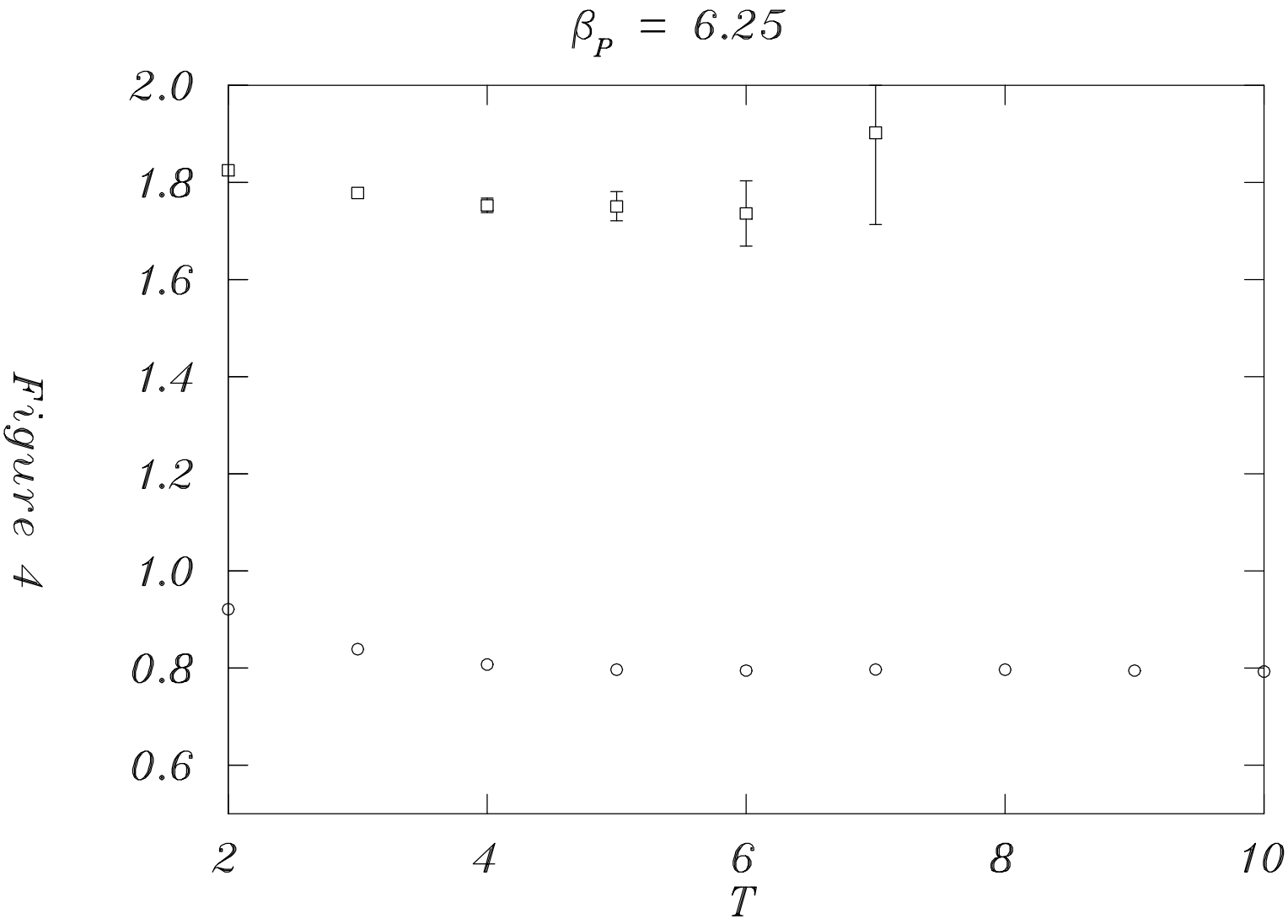

Figure 4

Hyperfine (MeV)
20
30
40
50
60
70
80
90
100
.00
.02
.04
.06
.08
.10
.12
.14
.16
α^2 (fm^2)

Figure 5